E19-2005-20

Kh. T. Kholmurodov[1], T. B. Feldman[2,3],
M. A. Ostrovsky[2]

# MOLECULAR DYNAMICS SIMULATION AND EXPERIMENTAL STUDIES ON THE VISUAL PIGMENT RHODOPSIN: MULTIPLE CONFORMATIONAL STATES AND STRUCTURAL CHANGES

Submitted to the Proceedings of the International Workshop MSSMBS'04 «Molecular Simulation Studies in Material and Biological Sciences», September 9–11, 2004, JINR, Dubna, Russia

[1] E-mail: mirzo@jinr.ru
[2] Biochemical Physics Institute, Russian Academy of Sciences, Moscow, Russia
[3] E-mail: feldman@sky.chph.ras.ru

Холмуродов Х. Т. и др.
E19-2005-20

Молекулярно-динамическое моделирование и экспериментальное изучение зрительного пигмента родопсина: множественность конформационных состояний и структурные изменения

На основе МД-моделирования с помощью суперкомпьютера и машины специализированного назначения «MDGRAPE-2» исследовались структурные конформационные изменения и динамическое поведение молекулы родопсина. Вычислены RMSD (среднеквадратичные отклонения) структуры родопсина с (11-*cis*) хромофорным ретиналем, построена микроскопическая (атомно-молекулярная) картина процессов, происходящих в т.н. области «белкового мешка», окружающего хромофорный ретиналь, проведено сравнение мобильности спиралей родопсина в областях бета-ионового кольца и шиффового основания. Одним из наиболее существенных моментов является то, что относительные отклонения спиралей родопсина коррелируют с вращательной трансформацией ретинального хромофора, точнее, с вращением бета-ионового кольца внутри связующего пакета родопсина («белкового мешка»). С целью изучения первичных процессов фотолиза родопсина использовалась низкотемпературная абсорбционная спектроскопия. Структурные и конформационные свойства родопсина, полученные на основе расчетов моделирования и эксперимента, указывают на существование множественных конформационных состояний ретинального хромофора внутри родопсина. Основными выводами из полученных результатов МД-моделирования и спектральных анализов являются: 1) наиболее вероятное, предпочтимое, состояние хромофора (11-*cis* ретиналь) определяется белковым окружением; 2) белковое окружение изменяет конформацию хромофорного ретиналя.

Работа выполнена в Отделении радиационных и радиобиологических исследований ОИЯИ.

Препринт Объединенного института ядерных исследований. Дубна, 2005

Kholmurodov Kh. T. et al.
E19-2005-20

Molecular Dynamics Simulation and Experimental Studies on the Visual Pigment Rhodopsin: Multiple Conformational States and Structural Changes

Based on the MD simulations with a supercomputer and the special-purposes MDGRAPE-2 machine we have performed 3-ns MD calculations on the rhodopsin molecule and presented the structure analysis data for its dark-adapted state. We have fulfilled the RMSD (root-mean-square deviation) and structural analysis for the rhodopsin (with 11-*cis* retinal), generated the pictures of the atomic-scale processes for the binding pocket, surrounding the chromophore retinal, and compared the helical deviations for the beta-ionone ring and Schiff base linkage regions of the protein. The most remarkable point of our observations is that the rhodopsin helical distortions in the dark state are accompanied with the transformation of the retinal chromophore, viz. with the rotation of the beta-ionone ring inside the protein binding pocket.

The low-temperature absorption spectroscopy technique has been used to study the primary stages of rhodopsin photolysis. The structural transformation properties of rhodopsin were discussed in due course of the simulations and experimental observations. It is proposed that the appearance of more than one intermediate at each stage of rhodopsin photolysis reflects the existence of multiple conformational states of the retinal chromophore in rhodopsin molecule in the dark-adapted state. As a summary of our observations we suggest that the conformational dynamics of the opsin helices determines the most probable chromophore (11-*cis* retinal) configuration, so that a favorable retinal conformation has to be adjusted by the protein surroundings.

The investigation has been performed at the Veksler and Baldin Laboratory of High Energies, JINR.

Preprint of the Joint Institute for Nuclear Research. Dubna, 2005

## INTRODUCTION

Visual pigment rhodopsin is the only light-sensitive protein in the disk membrane of the rod outer segment. This molecule belongs to a seven transmembrane helical protein receptor, known as G-protein-coupled receptors family. In Fig. 1 the ribbon structures of rhodopsin with retinal chromophore (twin structure model) are shown.

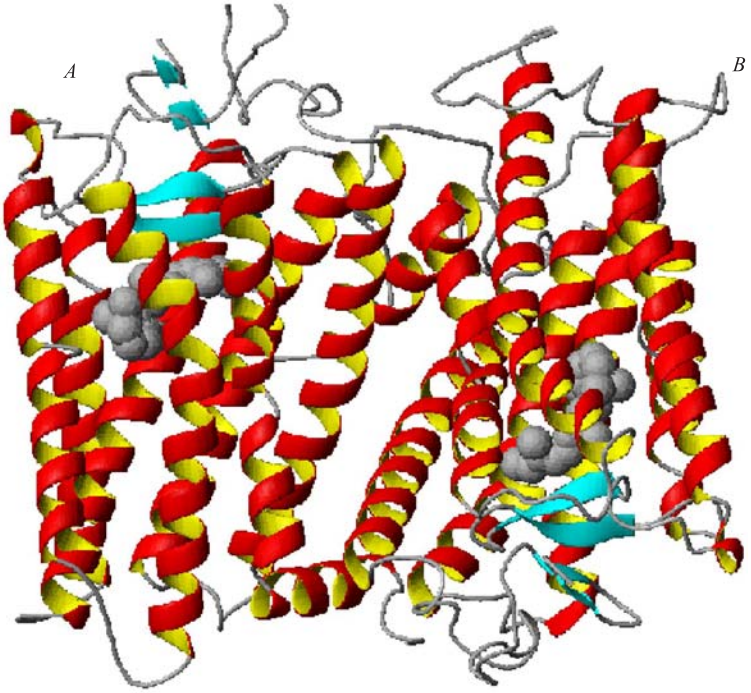


Fig. 1. Ribbon structure of the rhodopsin with the retinal chromophores: the retinal polyene chains are drawn by balls. The twin structure model (left — chain *A*; right — chain *B*) was constructed using a refined crystal structure of the rhodopsin (PDB entry 1HZX; Teller et al., 2001; Palczewski et al., 2000)

Rhodopsin consists of 11-*cis* retinal chromophore and protein opsin. 11-*cis* retinal covalently binds to the protein through a protonated Schiff base linkage, namely to the $\epsilon$-amino group of Lys-296 in the center of the helix VII (see Fig. 2, and Ref. [2]).

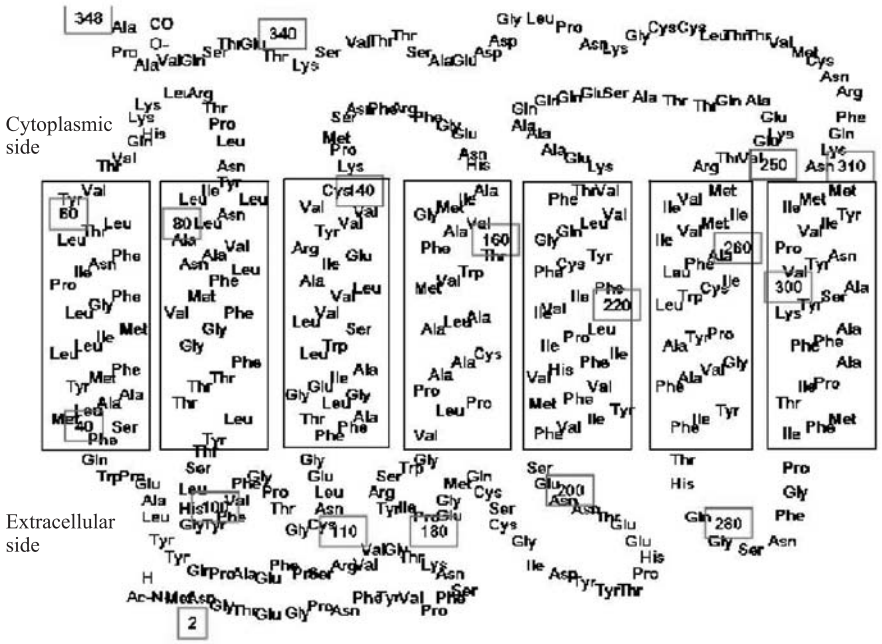


Fig. 2. Primary structure diagram with the positions of helices I–VII (from left to right) of rhodopsin protein is shown (Ovchinnikov et al., 1982; Teller et al., 2001; Palczewski et al., 2000)

Light isomerizes the 11-*cis* retinal to its all-*trans* form, that is followed by series of protein conformational changes. Rhodopsin is transformed into its activated state, which interacts with G-protein and initiates an enzyme cascade leading to the visual transduction. Finally, the all-*trans* retinal moves from the opsin chromophore site. This process is known as rhodopsin photolysis.

Spectroscopic methods have been extensively applied to the study the reactions following rhodopsin light excitation (see Fig. 3 for a schematic representation). One way to characterize the intermediates is to trap them at low temperatures [2, 3]. This approach led to the classical bleaching scheme (max values in nanometers):

rhodopsin (Rh) (498) → bathorhodopsin (Batho) (542) →
lumirhodopsin (Lumi) (497) → metarhodopsin I (Meta I) (480) →
metarhodopsin II (Meta II) (380).

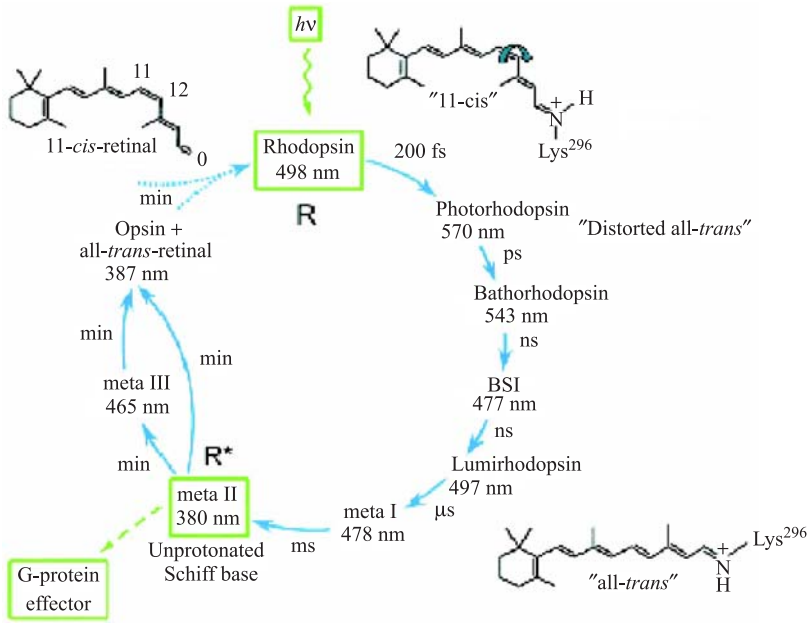


Fig. 3. Photocycle of rhodopsin with spectroscopically detected intermediates. (From: Ernst O. P. and Bartl F. J. Active state of Rhodopsin. Chem. Bio. Chem. 2002. V. 3. P. 968–974)

Time-resolved spectroscopy of rhodopsin with femtosecond resolution had allowed identifying the new first product of rhodopsin photolysis, namely photorhodopsin (PhotoRh) (max 585) [4, 5, 6]. Other time-resolved measurements, of up to 1 ms duration, reveal a new intermediate, called blue-shifted intermediate (BSI) [1]. The following reaction scheme was proposed and today is under consideration:

$$\text{Rh (498)} \rightarrow \text{PhotoRh (585)} \rightarrow \text{Batho (542)} \longleftrightarrow \text{BSI (477)} \rightarrow \text{Lumi (497)} \rightarrow \text{Meta I (480)} \rightarrow \text{Meta II (380)}$$

Recently resolved crystal structure of rhodopsin provides detailed structural information on the interactions between the retinal chromophore and its surrounding residues [7]. These data became a basis for the Molecular Dynamics Simulations to calculate the rhodopsin dark-adapted state as well as the possible pathways and structures of intermediates after rhodopsin photoexcitation.

The correlation of rhodopsin conformational dynamics and activation process of rhodopsin at later stages are the most challenging targets for computer mole-

cular simulations. The relative movement of the rhodopsin helices, for example, could be a part of the rhodopsin light-activated photocycle [34, 43]. The experiments revealed that a relative movement of the rhodopsin helices (for example, a movement of helix VI relative to other helices) plays a key role in the rhodopsin activation [59, 60]. This evidently motivates the extremely time consuming atomic modeling of rhodopsin. It has been considered that large-scale motion of rhodopsin protein may be a common dynamical motion for other alpha-helical G-protein receptors [34, 61].

In today's molecular modeling, rhodopsin conformation and its photo-induced isomerization were mostly studied by the conventional and quantum-mechanical molecular dynamics (MD and *ab initio* QM/MM) methods [34, 40–43]. Although the *ab initio* QM provides a basic insight into the mechanisms of the rhodopsin conformation changes, the actual reaction paths can deviate due to thermal fluctuations, reaction excess energies, etc. Through the MD simulation, on the other hand, the characteristic of the incoherent kinetic and dynamics can be captured directly [43]. Consequently, conventional MD method represents itself as a more adequate approach for providing a detailed picture of the atomic-scale processes of rhodopsin conformation. Many of the recent MD simulations were aimed to describe rhodopsin isomerization process and its conformational relaxation steps [40, 42, 43]. In [43], for example, MD simulations were performed on the rhodopsin protein embedded in a lipid bilayer and water environment. The retinal chain was isomerized around $C_{11} = C_{12}$ double bond, changing its conformation from 11-*cis* to all-*trans*, in accordance to the experimental observations [44–49]. It is worth noting, however, that the nature of non-reaction transformation, molecular mechanisms or conformational changes of rhodopsin protein is still unknown. The dynamics of rhodopsin conformation, its photoisomerization processes or transition states may essentially be influenced by the environmental conditions (opsin + solvent) [38, 41].

In Figure 4 the schematic diagrams of the retinal binding pocket for the rhodopsin protein are presented. It is worth noting that the analysis of the electron density data on the 11-*cis*-retinal chromophore and trans-membrane helices [30, 36] provides some preliminary picture of the intramolecular interactions in the rhodopsin protein. The structural conformations of rhodopsin essentially determine its function as a light-activated receptor.

The retinal binding site or salt bridges in rhodopsin are evidently correlate with the activation mechanism of the protein. The rhodopsin activation is associated, for example, with a shift of the relative orientation of helices III and VI [34, 43]. The Schiff base group and Glu-113 binding stabilize the connection between helices III and VII, the disruption of this binding site activates of rhodopsin at the absence of a retinal chromophore. In later stages of rhodopsin photolysis (META-I and META-II intermediates) the major conformational changes of rhodopsin are occured.

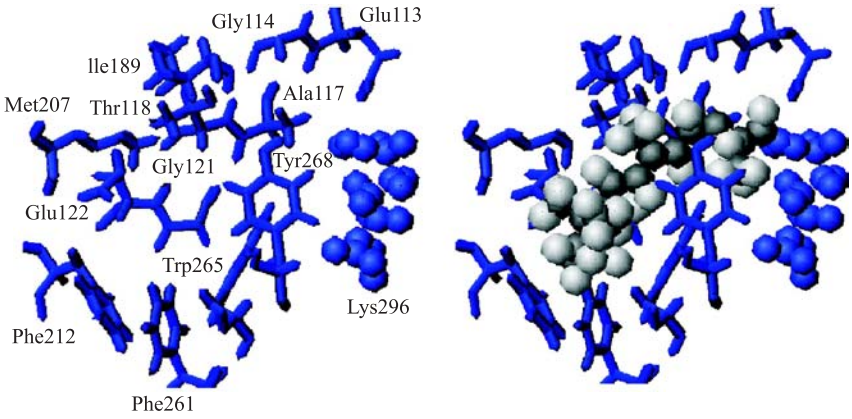


Fig. 4. The schematic diagrams of a retinal binding pocket in the rhodopsin structure are shown. The chromophore retinal chain and Schiff base linkage are drawn by balls. The position of beta-ionone ring of the retinal polyene chain is left-hand side

However, many uncertainties regarding the pathways of the rhodopsin conformation after photoexcitation still remain. Actually the current scheme of rhodopsin photolysis is that as it is represented above. Nevertheless, some papers discuss the existence of two or even three forms of rhodopsin intermediates on each stage of photolysis [8–12]. By other words, a multiple conformational state of visual pigment rhodopsin on different stages of its photolysis is quite possible to exist. The recent NMR spectroscopic data and Density functional theory calculations had shown the existence of two conformational forms of beta-ionone ring relative to the chromophore (6-s-*cis*-11-*cis*-retinal and 6-s-*trans*-11-*cis*-retinal), which populate protein pocket in the native dark state of rhodopsin [13, 14]. Perhaps, the above conformational states may generate different interactions with rhodopsin helices, leading to multiple intermediate states on each stage of rhodopsin photolysis. Thus, we had applied a complex approach to investigate the primary stages of rhodopsin photolysis, using a low-temperature technique and the rhodopsin dark-adapted state through the Molecular Dynamics Simulations.

## 1. MD SIMULATIONS ON RHODOPSIN STRUCTURAL CONFORMATION

### Simulation Details

We simulated the bovine rhodopsin in the dark-adapted state. The dynamics of rhodopsin conformation for dark-adapted state we examined through the

considerations: 1) rhodopsin without retinal; 2) rhodopsin with 11-*cis* retinal. A molecular model was constructed from the refined rhodopsin crystal structure as is shown in Fig. 1. In the MD simulations we use only one chain (molecule $A$) from the possible twin structure [36, 37]. The missing amino acids 236–240 and 331–333 were inserted using the MOE software package for biomolecular simulations [62]. The molecular mechanics (MM) and MD simulations on rhodopsin were performed with an explicit water solvent (see Fig. 5). Two set of MD simulations (viz. cutoff and no cutoff calculations) were performed with the program package AMBER [28, 63].

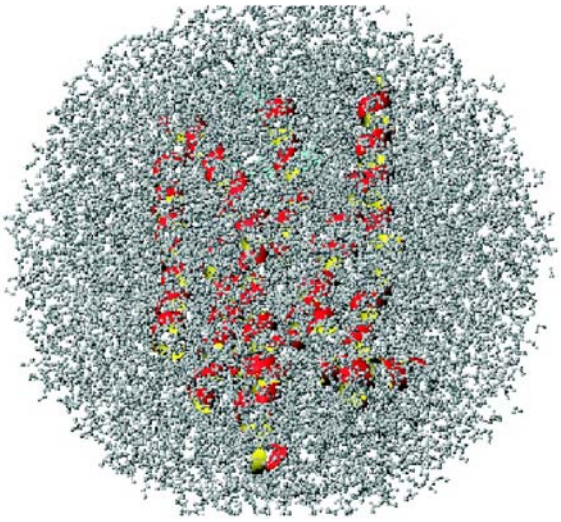

Fig. 5. The equilibrium configuration of rhodopsin protein is shown. The molecular mechanics and molecular dynamics simulations of rhodopsin were performed with a water solvent (the solvent TIP3P water molecules are drawn by small balls)

We have used the program package AMBER 5.0 (Parm94, cutoff method) [63] and modified version of AMBER 7.0 (Parm96, no cutoff method) for a special-purpose computer MDGRAPE-2 [64–66]. The all-atom force field of Cornell et al. [67] was used in the MD simulations. A system was solvated with TIP3P molecules [68] generated in a spherical (non-periodic) water bath. The system temperature was kept constant by using the Berendsen algorithm with coupling time of 0.2 ps [69]. Only bond lengths involving hydrogen atoms were constrained using the SHAKE method [70]. The cutoff distance of non-bonded interactions was 14 Å; for the MDGRAPE-2 all interactions were calculated. The integration time step in the MD simulations was 1 fs and the rhodopsin dynamics was studied for the $3{\cdot}10^6$ steps (3-ns state). The simulation procedures were the same in all calculations [50, 51]. Firstly, for each system a potential energy

minimization was performed on an initial state. Next, the MD simulation was performed on the energy-minimized states. The temperatures of the considered systems were gradually heated to 300 K for and then kept at 300 K for the next 3 million time steps. The trajectories at 300 K for 3 ns were compared and studied in detail. The result of simulations and images of simulated proteins were analyzed by RasMol [71] and MOLMOL [72] packages.

## Simulation Results

***Rhodopsin without Retinal.*** In this consideration all kinds of interactions inside the rhodopsin pocket and the solvent environment for the chromophore retinal were neglected. Firstly, we present the results for the rhodopsin RMSD (root-mean-square displacement) changes. In Figs. 6 and 7 the RMSD for a total rhodopsin structure domain and for each of helices I–VII are shown.

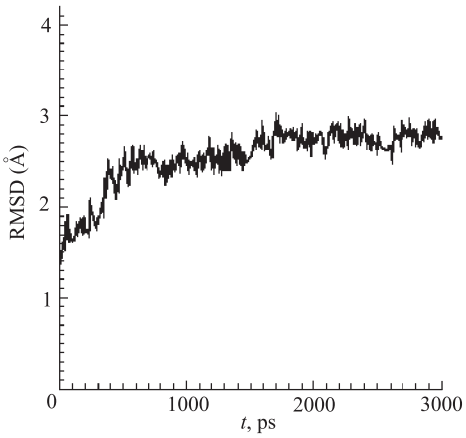


Fig. 6. The RMSD for the rhodopsin total structure is shown

The RMSD values were evaluated for only the backbone atoms of the helices. The RMSD of the total rhodopsin structure, as is seen from Fig. 6, has kept around 4.5 Å, indicating on a structural stability during 3.0-ns simulations. With regard to a selected helix (Fig. 7) we observe a relative movement of helices; displacement of the rhodopsin helices has different behavior. Helices I, III and V exhibit the highest deviations from the reference structure.

In Fig. 8 the superposition of the representative structures is presented at 3-ns state. Figure 8 shows the largest displacements from the reference structure for helices III and V. The largest differences are seen in the cytoplasmic region of the helices; the extracellular ends show slight movement. Some reported MD results indicate, for example, the largest RMSDs for helices I, V and VI or helices IV,

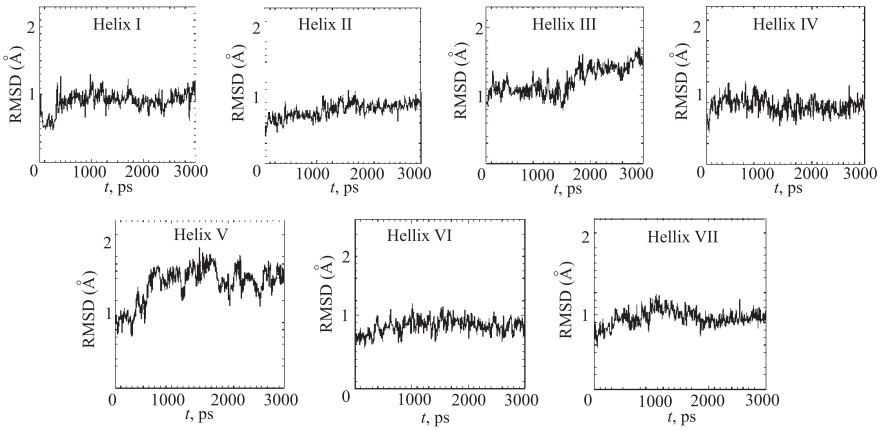


Fig. 7. The RMSD values calculated for each of rhodopsin helices I–VII are presented. (Free retinal state, no interatomic interactions for the retinal chromophore have been included). Helices I, III and V show the highest deviations from the reference structure

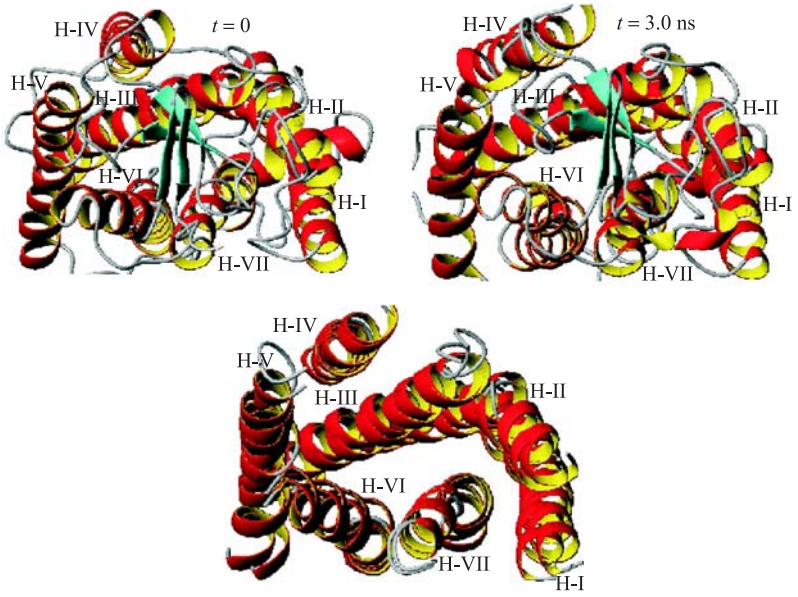


Fig. 8. The initial and final (3 ns) rhodopsin structures are shown (top). The superposition of the representative structures are displayed (bottom). The largest displacement from the reference structure is seen for helices III and V, respectively

V and VI [34,59,60]. It is worth noting that the spin-label experiments show the movement of the cytoplasmic part for helices II, VI and VII [26,27,43,61].

***Rhodopsin with 11-$cis$ Retinal.*** Next, we simulated the rhodopsin conformation dynamics with the inclusion of the 11-*cis* retinal at the start of runs. In Figs. 9 and 10 the RMSD results for the rhodopsin total structure domain and for each rhodopsin helices are presented.

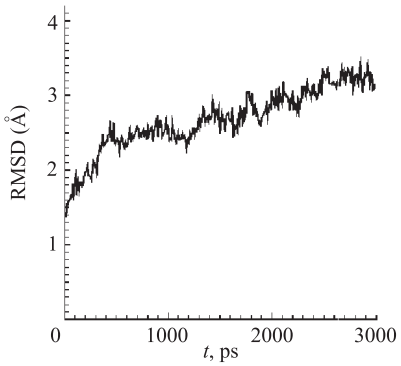


Fig. 9. The RMSD (root-mean-square displacement) of the total rhodopsin structure is shown. (The retinal in 11-*cis* conformation at the start of runs, all atomic interactions with rhodopsin and solvent)

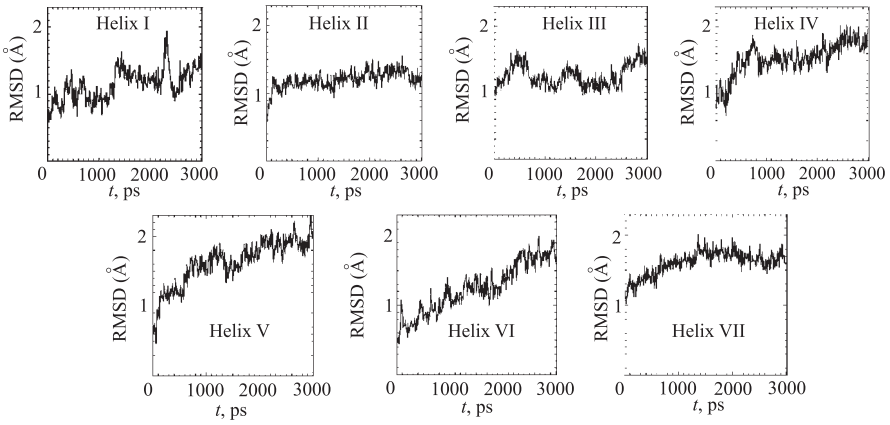


Fig. 10. The RMSD values calculated for each of helices I–VII are presented. (The retinal in 11-*cis* conformation at the start of runs, all atomic interactions in rhodopsin and solvent)

As is seen from Fig. 9, the inclusion of a small retinal chain into the whole dynamics does not influence the RMSD for the total rhodopsin structure. The RMSD during the 3-ns dynamics possesses the same average value of 4.5 Å, comparing Figs. 9 and 6, and the RMSD has the same behavior as in the absence

of the retinal chromophore. Nevertheless, with regard to a selected helix, the inclusion of the retinal chromophore results for all the RMSD values to change. From Fig. 10 the RMSD, separately estimated for each of helices, has clearly different behavior between the rhodopsin with 11-*cis* retinal and rhodopsin without retinal configurations. The comparison of the RMSD values are straightforward (see Fig. 10 and 7).

***Rhodopsin Conformation in the Dark-Adapted State.*** In Fig. 11 four sequential snapshots of the MD simulation are presented for rhodopsin ribbon structure with a retinal chromophore. The dynamical changes of the retinal chain inside the rhodopsin pocket are drawn separately with the balls.

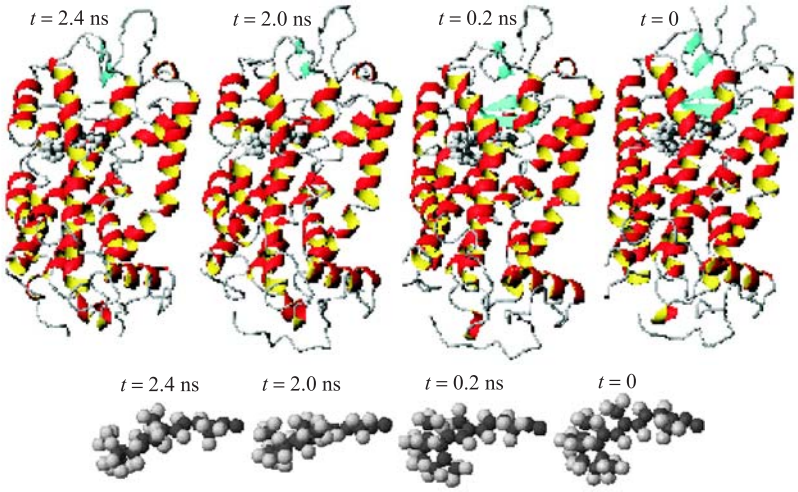


Fig. 11. Four sequential snapshots of the MD simulation. The rhodopsin ribbon structure and with retinal chromophore are shown (the dynamical change of the retinal chain is separately presented by the balls). The retinal polyene chain slightly rotates inside the rhodopsin pocket and it takes at final state (left picture, $t$ = 2.4 ns) a position perpendicular with regard to the initial state (right pictures, $t$ = 0)

From Fig. 11 we observe the rhodopsin helical deviations for both structural regions, viz., beta-ionone ring (left-hand side) and the Schiff base linkage (right-hand side). In comparison to the initial state (right pictures) the visibly high helical distortions have been seen at later stages (left pictures) within the frame of the 3-ns period. It is remarkable to note that rhodopsin helical distortions, as is seen from Fig. 11, have to be accompanied with a rotation of the beta-ionone ring.

In Fig. 12 the positions of the key amino acids within the binding pocket surrounding the retinal chain are shown. As is seen from Fig. 12 the retinal

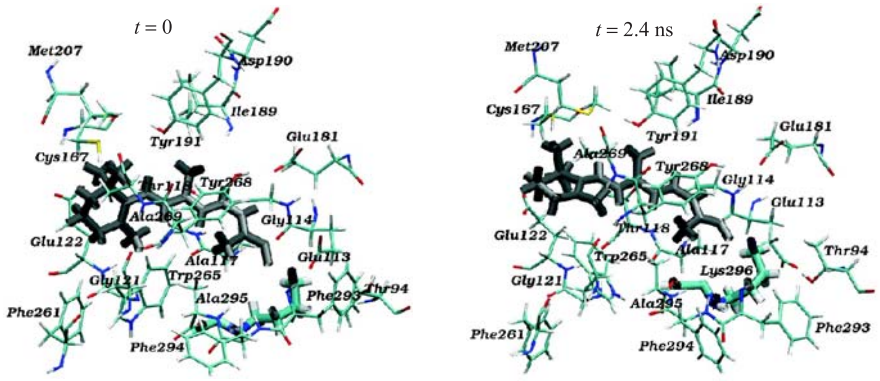


Fig. 12. A schematic representation of the retinal binding pocket region is shown at the initial ($t$ = 0) and later ($t$ = 2.4 ns) states. The positions of the key amino acids surrounding the retinal chain are drawn within the binding pocket. The retinal chain slightly transforms relative to the initial conformation

polyene chain during the dynamical changes inside the rhodopsin pocket has to be transformed in the beta-ionone region. The beta-ionone ring of the retinal chromophore at later stages (that is in the frame of 3-ns period) takes a position perpendicular with regard to that at the initial state.

***Rotational Changes of the Beta-Ionone Ring.*** Let us look at the details of the atomistic pictures generated for rhodopsin and retinal conformation inside its binding pocket. In Fig. 13 we present the calculated rhodopsin structures at the initial and final (3 ns) states (shown from the cytoplasmic part).

In Fig. 13 we observe that the structural changes occur for all helices and in both parts of the rhodopsin protein (viz., the Schiff base linkage — right-hand side, and beta-ionone ring — left-hand side). The visibly significant conforma-

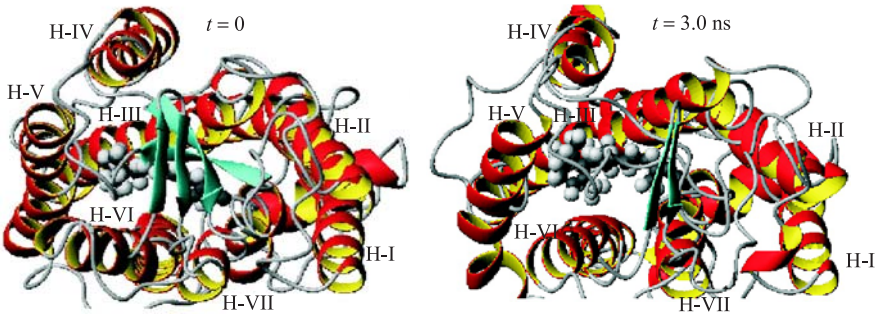


Fig. 13. The initial and final ($t$ = 3 ns) rhodopsin ribbon structures are presented (views are shown from the cytoplasmic side). The retinal chain is drawn by balls. The structure of the beta-ionone ring in comparison with the initial state became more planar with regard to helix III of the protein. At the final state helix VI reaches a closer position to the retinal chromophore

tional changes have been observed in the beta-ionone region. It is easy to see that the beta-ionone ring in course of its dynamics takes a more planar form relatively to helix III. Also helix VI in the final state reaches a more close position to the retinal chromophore. To enlighten the mechanisms underlying these conformational changes, a number of dynamical movies for the rhodopsin + retinal chromophore + water solvent were generated; the different structural positions and views were compared. The structural observations are summarized in the following three sets of the pictures (Figs. 14–16).

In Fig. 14 we see that the rotational changes of the beta-ionone region originate at the time of 0.3–0.4 ns from the start of the simulations (side view — the

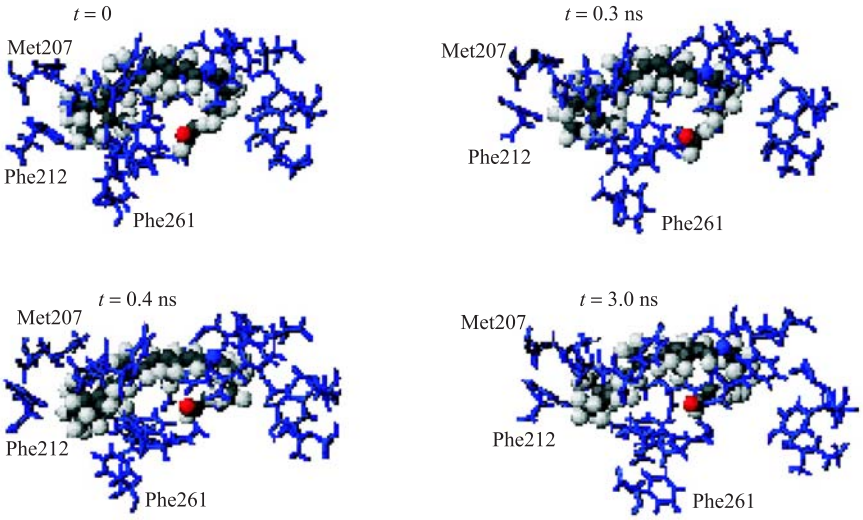


Fig. 14. The conformation of the retinal chain and positions of the key amino acids inside the rhodopsin binding pocket are shown. The rotational changes of the beta-ionone region originate at the interval 0.3–0.4 ns. Simultaneously within this temporal interval residue Phe-261 changes its position in relation with the retinal chain to an opposite site. The orientational change of the residue Phe-261 is seen to be accompanied with the rotation of the beta-ionone region

same as in Fig. 11). Within this time interval we observe the orientational changes of the amino acid residue Phe-261 (H-VI): this residue changes its position to an opposite site of the retinal chain. From our simulation we have found that the orientation of the residue Phe-261 occurs within a short interval (0.3–0.4 ns) and this is clearly accompanied by the rotation of the beta-ionone ring.

Starting from this point (at 0.3–0.4 ns) the beta-ionone ring keeps its conformation almost planar with regards to helix III (until the end of simulations, for about 2.6 million MD-time steps!). Thus, the Phe-261 orientational change

may probably initiate the retinal conformation change inside its binding pocket. However, in formation of the retinal conformation other amino acid residues or atomic sites may be involved. It is worth noting that retinal binding pocket is large and it is enough flexible to accommodate various chromophores.

In Fig. 15 we present a competition of the two amino acid residues (viz. Phe-212 and Ala-269) to be accommodated around the beta-ionone region (view from cytoplasmic part — the same view as in Fig. 13). Until the temporal point

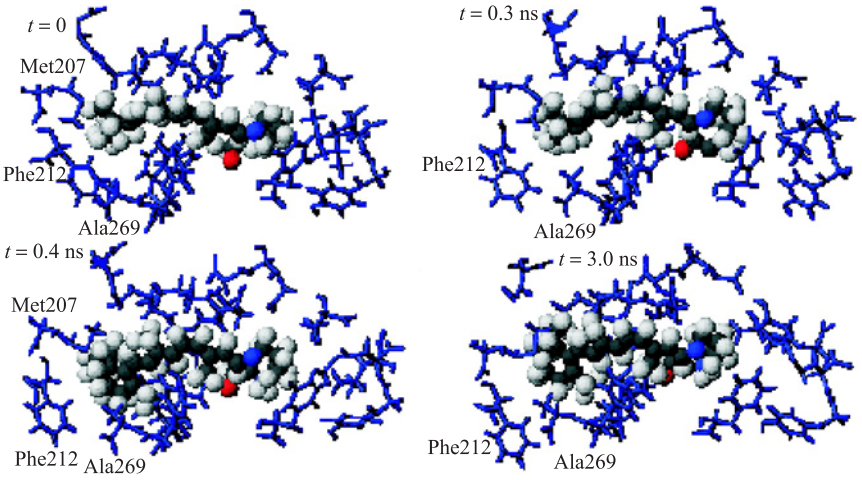


Fig. 15. The conformation of the retinal chain and key amino acid positions inside the rhodopsin binding pocket are shown (view from the cytoplasmic part of rhodopsin protein, the same as in Fig. 13). The positions of two amino acid residues, viz. Phe-212 and Ala-269, are compared. With the rotational changes of the beta-ionone ring at the interval of 0.3–0.4 ns the residue Ala-269 takes a closer position to the retinal site than that Phe-212

of 0.3–0.4 ns (say, a key point for the rotation of the beta-ionone ring) residues Phe-212 and Ala-269 are equidistantly positioned with regard to the polyene part of the chromophore. As rotation of the beta-ionone ring happens residue Ala-269 reaches a more close distance to the retinal (in beta-ionone region) than that of Phe-212. This perhaps results in the total helix VI displacement (to which the residue Ala-269 belongs) to be positioned closer to the chromophore retinal (in beta-ionone part).

In Fig. 16 a summary of the structural changes of the only retinal chromophore at different moments of time within 3-ns simulation is presented. The pictures in Fig. 16 display the retinal conformations for the same structural positions as described above (left — side view, the same as in Figs. 11 and 14; right — view from the cytoplasmic part, the same as in Figs. 13 and 15).

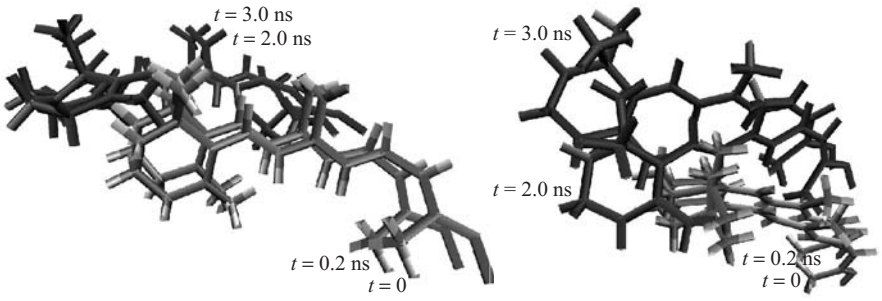


Fig. 16. The structural changes for the only retinal chromophore at the different moments of time are presented. The pictures display the retinal conformations on the same structural positions above (left — side view, the same as in Figs. 11 and 14; right — view from the cytoplasmic part, the same as in Figs. 13 and 15)

***The Details of the Rhodopsin Helical Movement.*** In this section we analyze rhodopsin conformation changes from the point of view of its interhelical movement. With regards to the structural conformation, the inclusion of a small retinal chain does not affect the RMSD average value. In other words, a small retinal chromophore, inside the rhodopsin and the embedded solvent environment, does not change the picture of atomic interactions. The RMSD, as is seen from Fig. 17, for the total rhodopsin structure has almost the same average value for both the rhodopsin with 11-*cis* retinal (solid line) and rhodopsin without retinal

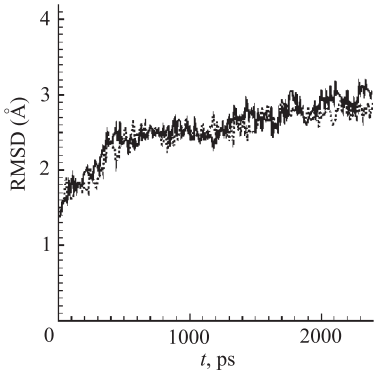


Fig. 17. The RMSD evolutions of the total structure for the rhodopsin with 11-*cis* retinal (solid curve) and rhodopsin without retinal (dotted curve)

(dotted line). From this comparison it is easy to observe that the RMSD in both considerations have the same dynamical behaviors.

It turns out that the inclusion of a retinal chromophore into the rhodopsin dynamics results in essential interhelical movement and conformational changes. Based on the RMSD analysis, we have estimated the helical changes for the rhodopsin with 11-*cis* retinal and rhodopsin without retinal. We consider the rhodopsin interhelical conformation in the following two regions: 1) the Schiff base linkage and 2) the beta-ionone ring.

***The Schiff Base Linkage Region.*** The Schiff base linkage region for the retinal chromophore includes helices I, II and VII. In Figs. 18–20 the structural conformations of these helices along with the retinal positions are displayed.

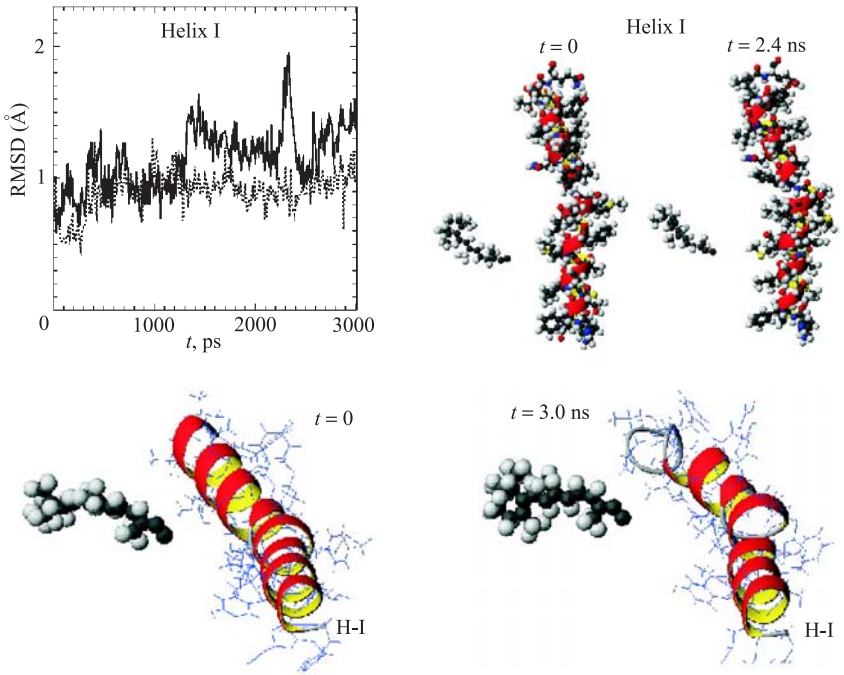


Fig. 18. The RMSD values of helix I (solid line — rhodopsin with 11-*cis* retinal; dotted line — rhodopsin without retinal) are displayed along with the positions of the helix in relation with the retinal chromophore (top snapshot — the distance view; bottom — view from the cytoplasmic side)

From Fig. 18 we observe that the RMSD for helix I (solid line for rhodopsin with 11-*cis* retinal) follows a nonlinear dynamics. Starting with a monotonic change at $t = 0$, the behavior of the RMSD becomes non-monotonic with time. Its value jumps around the points $t = 1.5$ and 2.5 ns, indicating the temporal distortion of this helix. As is seen in Fig. 18, the distance between helix I and retinal chain (in polyene part) gradually increases. The rotational change of the

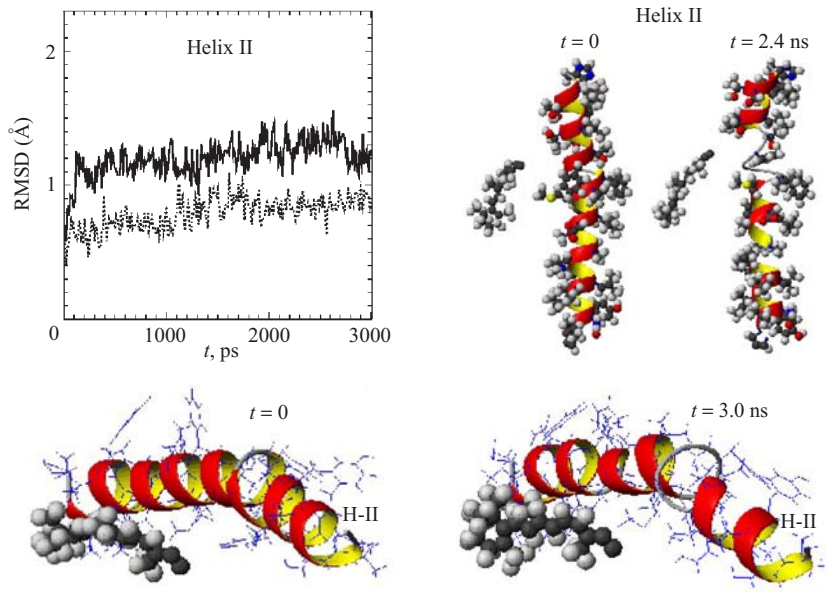


Fig. 19. The RMSD values of helix II (solid line — rhodopsin with 11-*cis* retinal; dotted line — rhodopsin without retinal) are displayed along with the positions of the helix in relation with the retinal chromophore (top snapshot — the distance view; bottom — view from the cytoplasmic side)

beta-ionone ring is directed normally to the axes of helix I (bottom snapshot). In Fig. 19 the comparison of the RMSD, the distance and the structures for helix II, are displayed. Helix II for the rhodopsin with 11-*cis* retinal has a higher deviation in comparison to the rhodopsin without retinal configuration. The positions of helix II and the polyene retinal chain change monotonically and the helical distortions are not so large. In Fig. 20 the comparison of the RMSD, the distance and the structural conformations of helix VII display visibly high deviations. To summarize the rhodopsin structural behavior in the Schiff base linkage region, we conclude that the retinal inclusion causes in this part of the protein the largest helical distortions. It is worth noting that all the rhodopsin structural changes described above occur within the retinal 11-*cis* configuration.

***The Beta-Ionone Ring Region.*** The beta-ionone region of the retinal chromophore includes the rhodopsin helices III–VI. The conformations of these helices along with the position of the retinal chain (in beta-ionone region) are presented in Figs. 21–24. For helix III (Fig. 21) the inclusion of the retinal chromophore seems helpful to maintain its original shape. Comparison of the RMSD (solid and dotted lines) shows that helix III does not deviate from its free

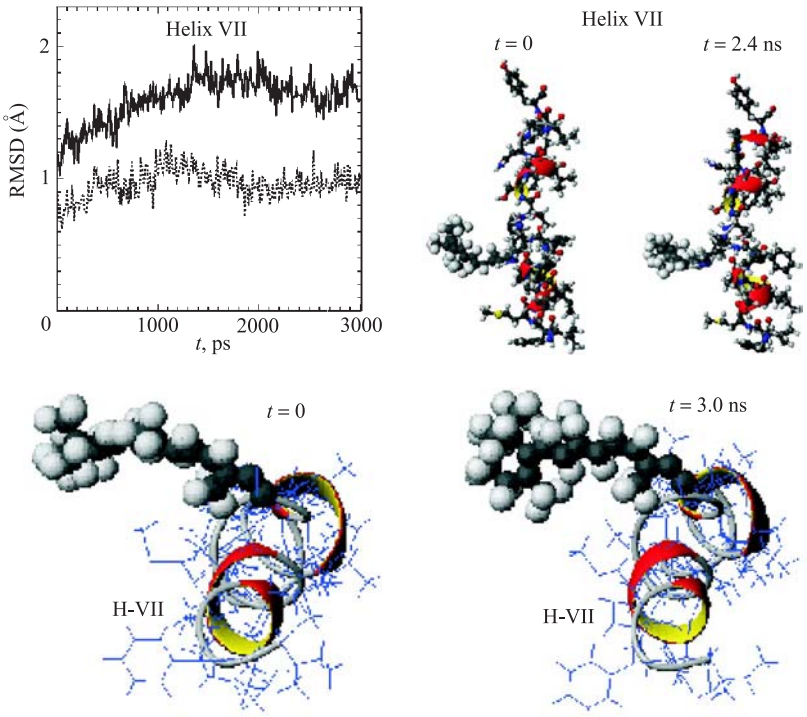


Fig. 20. The RMSD values of helix VII (solid line — rhodopsin with 11-*cis* retinal; dotted line — rhodopsin without retinal) are displayed along with the positions of the helix in relation with the retinal chromophore (top snapshot — the distance view; bottom — view from the cytoplasmic side)

form (at the absence of the retinal). The dynamical orientation of the retinal chain with time relatively to helix III becomes planar. Such a rotational change of the retinal chain seems to play a role in the structural stabilization of the helix. For helices IV and V (Figs. 22 and 23) the RMSD has greater values, if compared to the free form (solid and dotted lines). The distances from these helices to the retinal site (beta-ionone part) become shorter. In comparison to the initial state helices IV and V accommodate in the beta-ionone region more close positions to the retinal chromophore. In Fig. 24 the conformation behavior of helix VI is shown. The RMSD of helix VI increases within a simulation time. The increasing of the RMSD, however, does not accompanied with the distortion of helix VI outside of the rhodopsin binding pocket. On the contrary, helix VI takes a more close position to the beta-ionone ring of the retinal chain. To summarize,

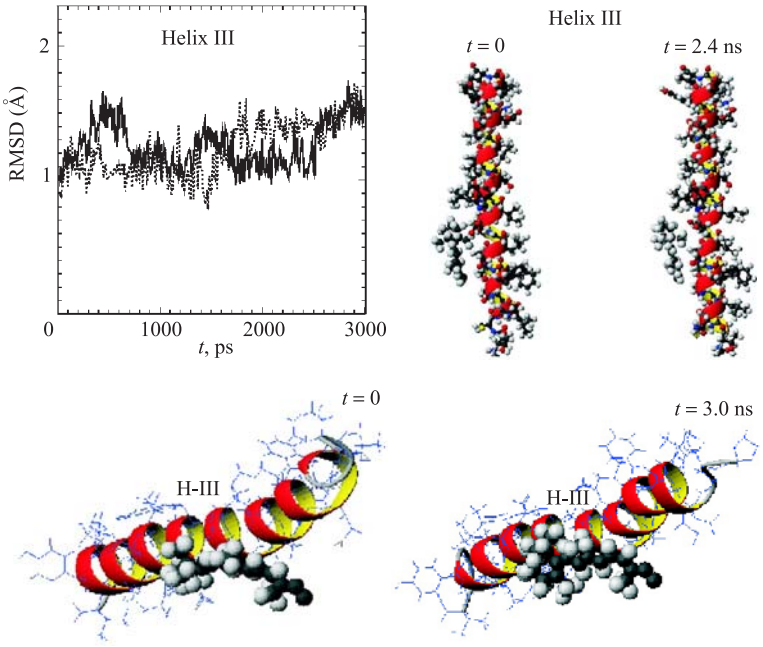


Fig. 21. The RMSD values of helix III (solid line — rhodopsin with 11-*cis* retinal; dotted line — rhodopsin without retinal) are displayed along with the positions of the helix in relation with the retinal chromophore (top snapshot — the distance view; bottom — view from the cytoplasmic side)

the rhodopsin conformation in the beta-ionone region has to be characterized by less helical distortions than that in the Schiff base linkage region.

## 2. LOW-TEMPERATURE SPECTROSCOPY STUDIES OF RHODOPSIN

### Spectral Measurements Procedures

***Rhodopsin Preparation.*** All the procedures were performed under dim-red light. Digitonin extracts of rhodopsin obtained from rod outer segments (ROS) suspension of bovine retina have been used [15]. The purity of obtained suspension was equal $A_{500\ nm/280\ nm}$ = 2.0–2.1. The ROS suspension was solubilized by 2% digitonin in $Na^{+}$- phosphate buffer (0.1 M, pH 7.4) contained 1 mM $MgCl_2$, 0.1 mM eDTA and 0.1 M hydroxylamine. All samples contained 65% of glycerol.

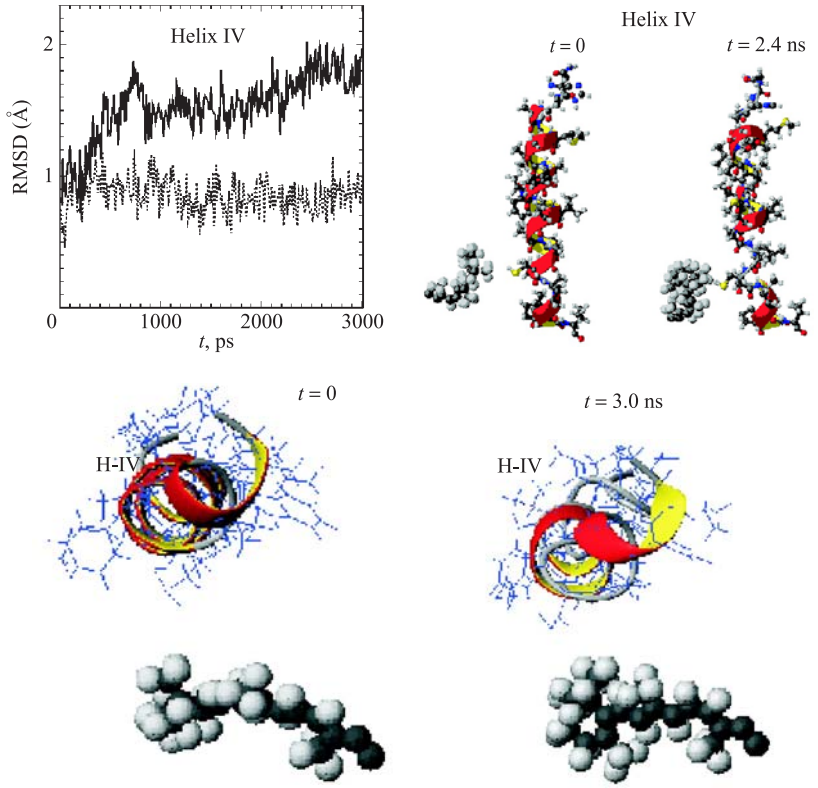


Fig. 22. The RMSD values of helix IV (solid line — rhodopsin with 11-*cis* retinal; dotted line — rhodopsin without retinal) are displayed along with the positions of the helix in relation with the retinal chromophore (top snapshot — the distance view; bottom — view from the cytoplasmic side)

***Spectral Measurements of Rhodopsin Transition at –155 °C and Above.*** The rhodopsin samples were irradiated at –155 °C by blue light at a wavelength of 436 nm as described in [12]. The sample was placed in a specially designed quartz Dewar flask [16]. Irradiation was performed with a DRSh-250 mercury lamp, using Hg-436 and 10-cm water filters. Steady-state absorption spectra were measured using a Shimadzu UV-1601PC spectrophotometer (Japan).

***Low-Temperature Spectroscopy Results.*** The rhodopsin was irradiated at –155 °C by blue light of the wavelength of 436 nm. As is known, the bathorhodopsin is stable at this temperature [3]. As a result of irradiation the steady state mixture of rhodopsin and bathorhodopsin is obtained. This mixture is contained near 70% of product with all-*trans* retinal [11]. The next classical product of

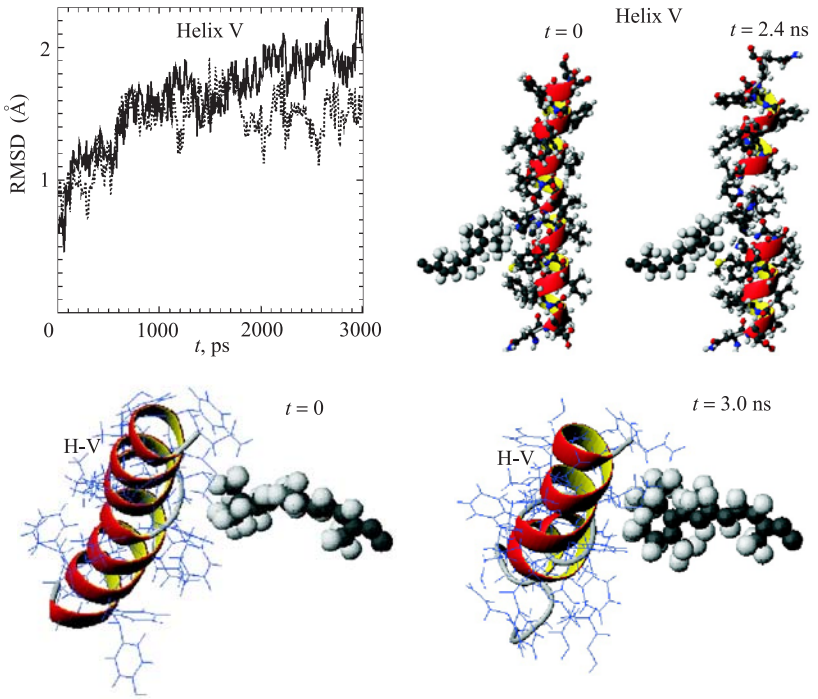


Fig. 23. The RMSD values of helix V (solid line — rhodopsin with 11-*cis* retinal; dotted line — rhodopsin without retinal) are displayed along with the positions of the helix in relation with the retinal chromophore (top snapshot — the distance view; bottom — view from the cytoplasmic side)

rhodopsin photolysis lumirhodopsin is appeared after raising of temperature to near –90 °C [17]. Both absolute and differential spectra that show this photoconversion are presented in Fig. 25.

However, if we have increased the temperature very slow by step 1–3 °C and recorded the spectra in the dark, we were able to observe during batho- to lumirhodopsin transition a simultaneous appearance more than one spectral products (Fig. 26). One can see a rise of absorption around 440 nm at temperature between –155 and –145 °C (Fig. 26, top — spectra *1–3*; bottom — spectra *1–4*). It cannot be lumirhodopsin, because absorption maximum of differential spectrum of lumirhodopsin is situated around 475 nm (Fig. 25, bottom — spectrum *2*). We will call this product as $D_{440}$ ($D$ means absorption maximum or minimum on differential spectrum).

Also, one can see a decrease of absorption minimum around 520 nm in the course of temperature rise. It means that an intermediate product with minimum

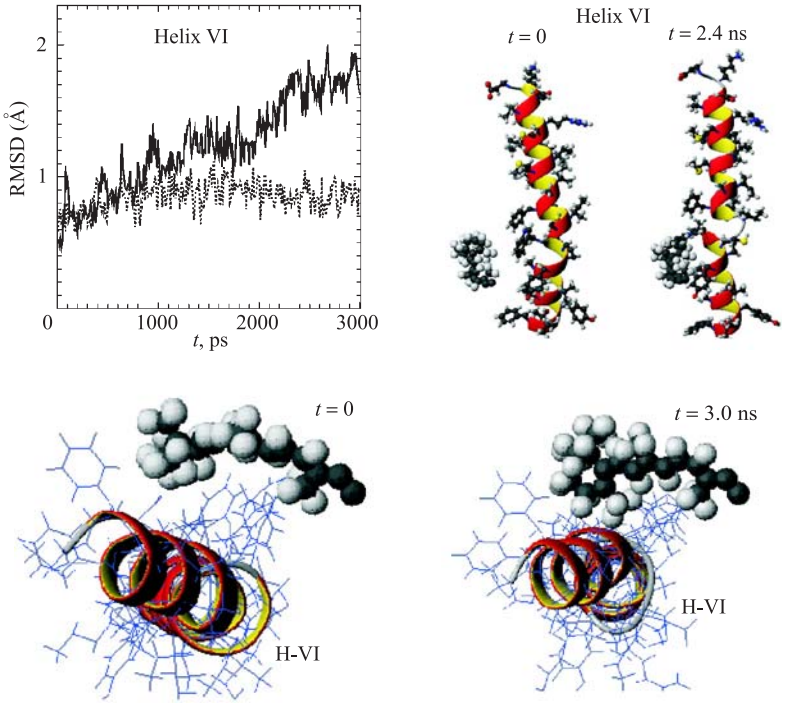


Fig. 24. The RMSD values of the helix VI (solid line — rhodopsin with 11-*cis* retinal; dotted line — rhodopsin without retinal) are displayed along with the positions of the helix in relation with the retinal chromophore (top snapshot — the distance view; bottom — view from the cytoplasmic side)

of absorption at 520 nm on the differential spectrum disappears. This $D_{520}$ nm product is not a bathorhodopsin, since its minimum of absorption on the differential spectrum situated at 555 nm (Fig 25, bottom — spectrum *2*). In fact, this $D_{520}$ nm product is a precursor of the other product with maximum of absorption at 440 nm. Indeed, one can see the isobestique point at 460 nm in the course of the $D_{520}$ nm product transition to the $D_{440}$ nm product. So, the existing of isobestique point supports our point of view that the $D_{440}$ nm product is formed from the $D_{520}$ nm product. Further temperature rise leads to formation of new products as can be seen from the appearance of absorption bands on the differential spectra at 475 and 555 nm. We suppose that these changes reflect the classical transition from batho- to lumirhodopsin. One should stress that in this case (at this higher temperature) the isobestique point is absent. It indicates again that the batho- to lumirhodopsin transition is not direct but more complicate process.

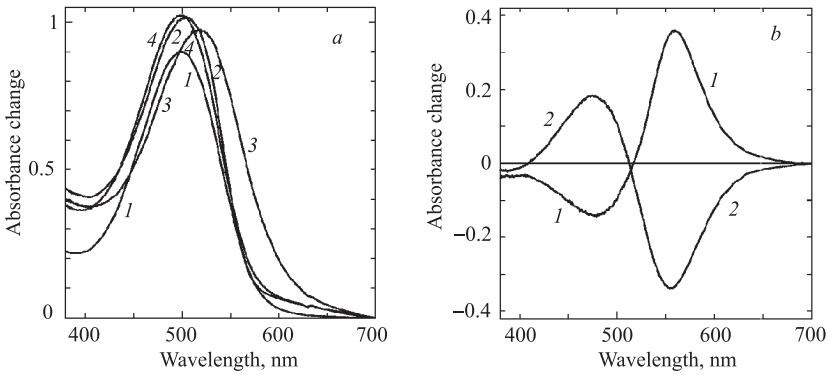


Fig. 25. Absorption spectra of rhodopsin and its photointermediates. *a*) Absolute absorption spectra. *1* — dark rhodopsin at 22 °C; *2* — dark rhodopsin at –155 °C; *3* — irradiated rhodopsin at –155 °C, 436 nm, 5 min (photostationary mixture of rhodopsin and bathorhodopsin); *4* — warmed photostationary mixture from –155 to –115 °C (stationary mixture of rhodopsin and lumirhodopsin). *b*) Difference spectra. *1* — rhodopsin to bathorhodopsin transition (*a* — curve 3 minus curve *2*); *2* — bathorhodopsin to lumirhodopsin transition (*a* — curve *4* minus curve *3*)

We can suppose that $D_{520} \rightarrow D_{440}$ and $D_{555} \rightarrow D_{475}$ transitions are occurred actually simultaneously (in parallel), and the first one — $D_{520} \rightarrow D_{440}$ is ahead of the second one — $D_{555} \rightarrow D_{475}$.

The differential spectra contain at temperatures from –110 °C and to higher only one maximum at 475 nm and one minimum at 555 nm. The shapes of these spectra become classical under such conditions. It described in literature as a batho- to lumirhodopsin transition [3, 17].

Based on the differential spectra analysis one can conclude that disappearance of $D_{520}$ and appearance of $D_{440}$ is not actually bathorhodopsin → lumirhodopsin transition ($D_{555} \rightarrow D_{475}$) or bathorhodopsin → BSI ($D_{555} \rightarrow D_{440}$). It is observed the appearance more than one, at least two, photointermediates on these early stages of rhodopsin photolysis. One can suggest the existence of parallel ways of rhodopsin photolysis.

## DISCUSSIONS

In the present work based on the MD simulation and spectral studies we have investigated the rhodopsin dynamical behavior and conformation properties.

We have performed 3-ns MD simulations on the rhodopsin and presented the structure analysis for the dark-adapted state. We have compared the dynamical properties of the rhodopsin protein in the following considerations: 1) Rhodopsin without retinal; 2) Rhodopsin with 11-*cis* retinal. In the former approach for the

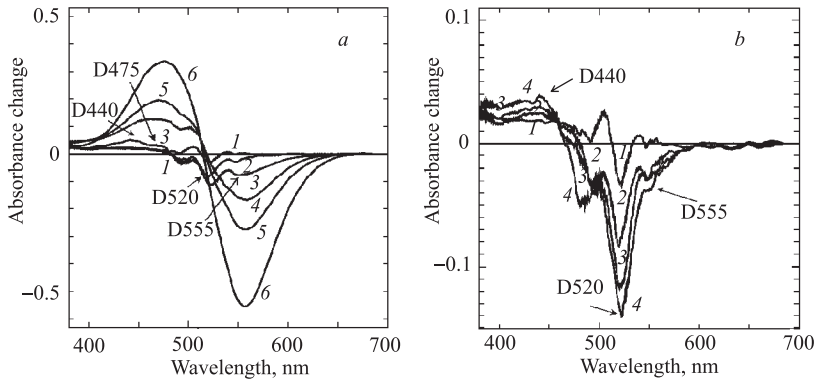


Fig. 26. Difference absorption spectra due to the thermal reaction of rhodopsin intermediates (after irradiation of rhodopsin at –155 °C, 436 nm, 5 min) are calculated by subtracting the absolute absorption spectrum (Fig. 25, curve *3*) recorded immediately after irradiation from the spectra recorded at later times after the irradiation in the course of a slow rise of temperature. *a*) Difference absorption spectra recorded in the temperature interval from –155 to –115 °C (spectra *1–6*). *1* — at –155 °C in 5 min after irradiation; *2* — at –145 °C in 15 min after irradiation; *3* — at –130 °C in 1 h after irradiation; *4* — at –130 °C in 2 h after irradiation; *5* — at –120 °C in 3 h after irradiation; *6* — at –115 °C in 3.5 h after irradiation. *b*) Difference absorption spectra recorded in the temperature intervals from –155 to –145 °C. *1* — at –155 °C in 5 min after irradiation; *2* — at –145 °C in 15 min after irradiation; *3* — at –145 °C in 20 min after irradiation; *4* — at –145 °C in 25 min after irradiation

retinal chromophore all kinds of interactions inside the rhodopsin pocket and with water solvent were neglected. The analysis of the RMSD (root-mean-square deviation) and generated structure images for the rhodopsin (without retinal) show a relative movement of rhodopsin helices, that possesses different behavior between the helices. Helices III and V of the rhodopsin exhibit the highest deviations from the reference structure. In the latter consideration for the rhodopsin (with 11-*cis* retinal) we generated the pictures of the atomic-scale processes for the binding pocket, surrounding the chromophore retinal, compared the helical deviations in the beta-ionone ring and Schiff base linkage regions of the protein. We have observed that the inclusion of small retinal chain into the whole rhodopsin dynamics (+ solvent) does not affect the RMSD behavior of the total rhodopsin structure. Within the 3-ns time step calculations the RMSD of the whole rhodopsin molecule (11-*cis* retinal) possesses the same average value and behavior as in the absence of the retinal chromophore. However, one should stress out that concerning a selected rhodopsin helix, the inclusion of the retinal changes all RMSD values and causes essential helical distortions.

The structural images were generated to display the conformation of each of the rhodopsin helices. The detailed structural configurations were separately

estimated for the beta-ionone ring and Schiff base linkage regions of rhodopsin. The Schiff base linkage region for the retinal chromophore includes helices I, II and VII. The RMSD of helix I shows a nonlinear dynamics, indicating the temporal distortion of the helix: the distance between helix I and the retinal chain gradually increases. The temporal positions of helix II and the retinal chain show that the helical distortion is not to be so large. The RMSD, distance and structural data of helix VII indicate a visibly high deviation. The beta-ionone region of the retinal chromophore involves helices III–VI of the rhodopsin. The inclusion of the retinal chromophore for helix III seems helpful to maintain its original shape. The comparison of the RMSD with helix III shows that the helix does not deviate as much as similar in the absence of the retinal. The orientation of the retinal chain with regards to helix III became a clearly planar, and that this rotational dynamics of the retinal chain probably plays an important role in the structural stabilization of the helix. For helices IV and V the RMSD shows significantly higher deviations, however the distances from these helices to the retinal site (in beta-ionone region) seem to become shorter. In comparison with the initial state, helices IV and V accommodate a more close positions relatively to the retinal chromophore. The RMSD calculated for helix VI increases within a long period of simulation time. The increasing of the RMSD, however, is not accompanied by the helical distortion; on the contrary, helix VI accommodates a close position to the retinal chain. It is worth noting that some reported MD results indicate the largest RMSDs for helices I, V and VI or helices IV, V and VI [34, 59, 60]. The spin-label experiments, for example, show the movement of the cytoplasmic part for helices II, VI and VII [26, 27, 43, 61].

It is remarkable that the rhodopsin helical distortions are accompanied by the rearrangement of the retinal chromophore, viz. with a tuning of the beta-ionone ring inside the protein binding pocket. From our simulation results we observed that within a short interval (0.3–0.4 ns) the beta-ionone ring changes its orientation along the retinal chain. It is worth noting that such reorientation, however, does not occur for different parts of the retinal chromophore simultaneously. In accordance to our RMSD data and generated animations (structure movies), from the start of the above time interval the oscillation of a retinal methyl group C20 could easily be distinguished as oscillation of a pendulum perpendicularly to the polyene chain. That is the C20 methyl possesses a higher amplitude if to compare the latter to other retinal groups. It seems that C20 methyl group swings up the whole chromophore molecule, helping the chromophore to change an arrangement in its local site and to reach a more favorable state. As the retinal reorientation occurs the different groups of the retinal chain preserve their oscillation peculiarities. One can easily observe the rotational type oscillations of the methyl groups C19 and C20 around the polyene chain (as oscillation of a pendulum), where C20 oscillates with a greater amplitude. At the same time, the oscillation of these methyl groups are not synchronized. One can propose an

assumption that these ocsillations may serve as a premise to or bringing to the strongly twisted retinal chain in the central region, from C10 to C13 [19–23], where this twist may be responsible for the initial ultrafast isomerization reaction. Moreover, as have been reported in [24], after the retinal photoisomerization large C20 rotation and translation toward H-V disrupt the interactions of H-V, H-VI, and H-VII with the core of rhodopsin and lead to receptor activation [24]. It is very likely that for the rhodopsin dark-adapted state the large mobility of C20 group, in comparison with the other chromophore fragments, may serve as prerequisitive for a large C20 rotation in the excited-state rhodopsin. It is obviously that such dynamical behavior of the retinal chromophore inside the chromophore pocket has governed by the only protein surrounding.

It is worth to note that the experiments provide the data, for example, for the position of the beta-ionone ring, and that it is mostly covered from the cytoplasmic side by the residues of helices III and VI (the residues Glu-122, Phe-261, Trp-265) [30, 36]. Helix III provides many of the side chains for the binding pocket (say, Glu-113, Gly-114, Ala-117, Thr-118, Gly-120, Gly-121) surrounding the retinal polyene chain. From the extracellular side the side chains of Tyr-268 and Ile-189 determine the position of the C9-methyl of the retinylidene group. Side chains from H-V and H-VI (residues Met-207, His-211, Phe-212 Tyr-268 and Ala-269) also surround the beta-ionone ring [36, 52–54]. Moreover, the retinal reorientation may initiate, on the other hand, the conformational rearrangement of the amino acid residues in the chromphore location site. From our simulation results we observed that within a short interval (0.3–0.4 ns) the beta-ionone ring changes its orientation in relation to the retinal chain. The beta-ionone ring at later stages takes more planar position with respect to helix III of the rhodopsin. Within this interval the amino acid residue Phe-261 simultaneously changes its orientation relatively to the retinal chromophore. The beta-ionone ring rotation changes the positions of two amino acid residues, Phe-212 and Ala-269. Starting from 0.3–0.4 ns the residue Ala-269 accommodates closer position to the chromophore retinal (in the beta-ionone site) than a key residue Phe-212 does. Thus, our RMSD and other structural data confirm once more the importance of the chromophore-protein interactions. At the same time, our results are indicating on some molecular mechanisms of the protein and chromophore arrangement, under which the rhodopsin molecule may have its function or will behave as a highly sensitive sensor with the high quantum (about 0.65) and isomerization speed (less 250 fs) [30, 36, 52–54].

Today the question about the truth retinal configuration in the chromophore site is one of the most arguing and discussed one. Unfortunately, the experimental structural (X-ray or NMR) data cannot provide an unique answer here. Thus, at the present several theoretical and experimental works with contradictory conclusions have to exist. For example, there have been several reported results regarding on the beta-ionone ring conformation relatively to the retinal chain.

Though it has been long assumed that the geometry is twisted 6-s-*cis* [21], a recent NMR [18] spectroscopic study has cast doubts on this and proposed that the conformation is derived from 6-s-*trans* instead. Moreover, it was discussed the existence of two conformations of the beta-ionone ring simultaneously. Density functional theory calculations in [14] assumed that protein pocket tolerates both conformations, 6-s-*cis* and 6-s-*trans*, where 6-s-*cis* is a more stable conformer than 6-s-*trans* and compound 3 : 1 equilibrium population at room temperature. The experimental study confirmed this prediction [13]; the authors based of NMR spectroscopic data concluded that the binding pocket is populated by two conformational states. A minor component comprising about 26% and corresponding possibly to a twisted 6-s-*trans* form and a major component which the authors identify as the 6-s-*cis* conformer. Moreover, in [22] on the basis of the PM3-SDCI calculations the authors suggest that 6-s-*trans* geometry is preferred in the binding pocket under conditions when interactions with the protein environment are included. In recent studies [23], starting with models built from the X-ray data of the 2.6 Å structure [37] and their own of the 2.2 Å structure, QM/MM MD simulations have been performed. The obtained result supports the 6-s-*cis* form with substantial negative twist.

From our data presented above we also conclude that at the 3-ns MD calculated state 6-s-*cis* seems to be the most preferable conformer. At the same time this conformational state of rhodopsin (with a nonplanar distorted and twisted retinal) differs from that we have used [36] as initial state at the start of the MD simulations. In this rhodopsin state we have a retinal with a planar structure, like free 6-s-*cis*-11-*cis*-retinal conformation. In spite of the fact that our theoretical calculations are only model, we can suppose that the initial conformational state of the retinal can make a physiological sense. It is well known that the free retinal in solution usually takes a similar to planar structure. Under physiological conditions the retinal chromophore brought from pigment epithelium to the rhodopsin molecule, during a regeneration process, in a structure like to planar. From our simulation data we see that the rhodopsin helical distortions helping retinal to be transformed into the nonplanar distorted or twisted conformation. Thus, from our results we suppose that the initial 6-s-*cis* (like free retinal) transformation requires some initial «re-stabilization» time (say, 0.3–0.4 ns) to occur. During this time interval the rhodopsin helical fluctuations push the retinal to be reoriented in a manner as described above. So, it is not excluded that the existence of two states of rhodopsin molecule (characterized by two different conformational states of the retinal chromophore) could be possible. These two different forms of rhodopsin molecule may possess different spectral properties and behaviors after the rhodopsin excitation.

Our simulation data described above are in good agreement with our experimental studies on low-temperature spectroscopy of rhodopsin. Low-temperature spectroscopy results allow one to presume that there are more than one interme-

diate at each stage of rhodopsin photolysis. It is very possible that the rhodopsin photolysis is not a linear process. Probably, there are parallel ways. The product with maximum of absorption at 440 nm is similar to the product known as a blue-shifted intermediate. It has been found in [1] that BSI is the intermediate, which is formed from bathorhodopsin and transformed to lumirhodopsin. In our case, it is clearly to see that this product is not formed from bathorhodopsin, but formed from the product that is appeared simultaneously with classical bathorhodopsin. It cannot be excluded that we have observed not one but two products on the early stage of rhodopsin photolysis that is produced from the two forms of chromophore conformation. In other words, one can proposed that there are multiple conformational states of the native dark rhodopsin. This approach is based on our simulation data and other data, concerning the conformation of the beta-ionone ring relative to the chromophore.

**NOTE.** From our point of view the theoretical and experimental data, concerning the existence of 6-s-*trans*-11-*cis*-retinal configuration in rhodopsin [13, 14, 18, 22], have to be considered as the subject for more detailed studies. On the one hand, it was shown that the planar 6-s-*trans* conformation of the free chromophore is energetically favored over the 6-s-*cis* conformation [25]. On the other hand, the binding site is not tight sufficiently [22], so this fact does not provide enough argument to conclude which conformation is favorable. We have also to remember that the retinal binding pocket is large and enough flexible to accommodate a variety of chromophores [36,43]. Thus, it is very likely that there is some possibility for the retinal rearrangement (say, from 6-s-*cis* to 6-s-*trans* configuration) or for the retinal embedding to be located properly in the opsin site in vivo. We consider the problems discussed above in today are open. Finally, considering the rhodopsin molecule as a template for other G-protein-coupled receptors (GPCRs) one could suppose that the retinal rearrangement inside the protein binding pocket might be a common process. That is the protein surrounding for other GPRCs may possess the same feature as rhodopsin to adjust for a related ligand or constitutive chain to take (like as chromophore retinal) the most favorable conformation.

## REFERENCES


1. *Hug S. J., Lewis J. W., Einterz C. M., Thorgeirsson T. E., Kliger D. S.* // Biochemistry. 1990. V. 29, No. 6. P. 1475–1486.

2. *Kandori H., Shichida Y., Yoshizawa T.* // Biochem. (Mosc). 2001. V. 66, No. 11. P. 1197–209.

3. *Yoshizawa T., Wald G.* // Nature. 1963. V. 197. P. 1279–1285.

4. *Peteanu L. A., Schoenlein R. W., Wang Q., Mathies R. A., Shank C. V.* // Proc. Nat. Acad. Sci. USA. 1993. V. 90, No. 24. P. 1176211766.

5. *Haran G., Morlino E. A., Matthes J., Callender R. H., Hochstrasser R. M.* // J. Phys. Chem. A. 1999. V. 103. P. 2202–2207.

6. *Kandori H., Furutani Y., Nishimura S., Shichida Y., Chosrowjan H., Shibata Y., Mataga N.* // Chem. Phys. Lett. 2001. V. 334. P. 271–276.

7. *Palczewski K., Kumasaka T., Hori T., Behnke C. A., Motoshima H., Fox B. A., Le Trong I., Teller D. C., Okada T., Stenkamp R. E., Yamamoto M., Miyano M.* // Science. 2000. V. 289. P. 739–745.

8. *Grellmann K.-H., Livingston R., Pratt D.* // Nature. 1962. V. 193. P. 1258–1260;

9. *Sasaki N., Tokunaga F., Yoshizawa T.* // Photochem. Photobiol. 1980. V. 32. P. 433–441.

10. *Einterz C. M., Lewis J. W., Kliger D. S.* // Proc. of the Nat. Acad. Sci. USA. 1987. V. 84. P. 3699–3703.

11. *Protasova T. B., Fedorovich I. B., Ostrovsky M. A.* // Light in Biology and Medicine. 1991. V. 2. P. 545–556.

12. *Fel'dman T. B., Fedorovich I. B., Ostrovskii M. A.* // Neurosci. Behav. Physiol. 2004. V. 34, No. 7. P. 735–42.

13. *Spooner P. J. R., Sharples J. M., Verhoeven M. A., Lugtenburg J., Glaubitz C., Watts A.* // Biochem. 2002. V. 41. P. 7549–7555.

14. *Sugihara M., Buss V., Entel P., Elstner M., Frauenheim T.* // Biochem. 2002. V. 41. P. 15259–15266.

15. *Smith H. G., Stubb G. W., Litman B. J.* // Exp. Eye Res. 1975. V. 20. P. 211–217.

16. *Krongauz V. A., Shifrina R. R., Fedorovich I. B., Ostrovskii M. A.* // Biofizika. 1975. V. 20, No. 2. P. 219–224.

17. *Yoshizawa T., Shichida Y., Matuoka S.* // Vision Res. 1984. V. 24, No. 11. P. 1455–1463.

18. *Grubner G., Burnett I. J., Glaubitz C., Choi G., Mason A. J., Watts A.* // Nature. 2000. V. 405. P. 810–813.

19. *Lin S. W., Groesbeek M., van der Hoef I., Verdegem P., Lugtenburg J., Mathies R. A.* // J. Phys. Chem. B. 1998. V. 102. P. 2787–2806.

20. *Verdegem P. J. E., Bovee-Geurts P. H. M., de Grip W. J., Lugtenburg J., DeGroot H. J. M.* // Biochem. 1999. V. 38. P. 11316–11324.

21. *Han M., Smith S. O.* // Biochem. 1995. V. 34. P. 1425–1432.

22. *Singh D., Hudson B. S., Middleton C., Birge R.* // Biochem. 2001. V. 40, No. 14. P. 4201–4204.

23. *Okada T., Sugihara M., Bondar A.-N., Elstner M., Entel P., Buss V.* // J. Mol. Biol. (in press).

24. *Patel A. B., Crocker E., Eilers M., Hirshfeld A., Sheves M., Smith S. O.* // PNAS. 2004. V. 101, No. 27. P. 10048–10053.

25. *Terstegen F., Buss V.* // J. Mol. Struct. (THEOCHEM). 1998. V. 430. P. 209–218.

26. *Pogozheva I. D., Kuznetsov V. A., Livshits V. A., Fedorovich I. B., Ostrovsky M. A.* // Biological Membranes. 1985. V. 2. P. 880–896 (in Russian).

27. *Pogozheva I. D., Kuznetsov V. A., Livshits V. A., Ostrovsky M. A.* // Biological Membranes. 1985. V. 2. P. 897–905 (in Russian).

28. *Weiner S. J., Kollman P. A., Nguyen D. T., Case D. A.* // J. Comp. Chem. 1986. V. 7. P. 230.

29. *Brooks B. R., Bruccoleri R. E., Olafson B. D., States S., Swanimathan D. J., Karplus M.* // J. Comp. Chem. 1983. V. 4. P. 187–217.

30. *Okada T. et al.* // J. Struct. Biol. 2000. V. 130. P. 73–78.

31. *Shieh T., Han M., Sakmar T. P., Smith S. O.* // J. Mol. Biol. 1997. V. 269. P. 373–377.

32. *Herzyk P., Hubbard R. E.* // J. Mol. Biol. 1998. V. 281. P. 741–747.

33. *Henderson R., Schertler G. F. X.* // Phil. Trans. R. Soc. Lond. 1990. V. 326. P. 379–389.

34. *Crozier P. S., Stevens M. J., Forrest L. R., Woolf T. B.* // J. Mol. Biol. 2003. V. 333. P. 493–514.

35. *Zrenner E.* // Science. 2002. V. 295. P. 1022–1025.

36. *Palczewski K., Kumasaka T., Hori T., Behnke C. A., Motoshima H., Fox B. A., le Trong I., Teller D. C., Okada T., Stenkamp R. E., Yamamoto M., Miyano M.* // Science. 2000. V. 289. P. 739–745.

37. *Teller D. C., Okada T., Behnke C. A., Palczewski K., Stenkamp R. E.* // Biochem. 2001. V. 40. P. 7761–7772.

38. *Kandori K., Shichida I., Yoshizawa T.* // Biochem. 2001. V. 66. P. 1483–1498 (in Russian).

39. *Pan D., Mathies R. A.* // Biochem. 2001. V. 40. P. 7929–7936.

40. *Humphrey W., Lu H., Logunov I., Werner H. J., Schulten K.* // Biophys. J. 1998. V. 75. P. 1689–1699.

41. *Tajkhorshid E., Baudry J., Schulten K., Suhai S.* // Biophys. J. 2000. V. 78. P. 683–693.

42. *Hayashi S., Tajkhorshid E., Schulten K.* // Biophys. J. 2002. V. 83. P. 1281–1297.

43. *Saam J., Tajkhorshid E., Hayashi S., Schulten K.* // Biophys. J. 2002. V. 83. P. 3097–3112.

44. *Warshel A.* // Nature. 1976. V. 260. P. 679–683.

45. *Birge R. R., Hubbard L. M.* // J. Am. Chem. Soc. 1980. V. 102. P. 2195–2205.

46. *Warshel A., Barboy N.* // J. Am. Chem. Soc. 1980. V. 104. P. 1469–1476.

47. *Tallent J. R., Hyde E. W., Findsen L. A., Fox G. C., Birge R. R.* // J. Am. Chem. Soc. 1992. V. 114. P. 1581–1592.

48. *Rohrig U., Guidoni L., Rotlisberger U.* // Biophys. J. 2002. V. 82. P. 223a.

49. *Choi G., Landin J., Galan J. F., Birge R. R.* // Biochem. 2002. V. 41. P. 7318–7324.

50. *Kholmurodov K., Ebisuzaki T.* // ICMS-CSW2004. Tsukuba, 2004. V. C4. P. 9–11.

51. *Kholmurodov K. et al.* // Phys. of Elem. Part. At. Nucl. 2003. V. 34. Part 2. P. 474–510.

52. *Sakmar T. P., Franke R. R., Khorana H. G.* // Proc. of the Nat. Acad. Sci. USA. 1989. V. 86. P. 8309–8313.

53. *Birge R. R.* // Biochem. Biophys. Acta. 1990. V. 1016. P. 293–327.

54. *Farrens D. L., Altenbach C., Yang K., Hobbell W. L., Khorana H. G.* // Science. 1996. V. 274. P. 768–780.

55. *Khorana H. G.* // Proc. of the Nat. Acad. Sci. USA. 1993. V. 90. P. 1166–1171.

56. *Gelther U., Kobilka B. K.* // J. Biol. Chem. 1998. V. 273. P. 17979–17982.

57. *Kuwata O., Yuan C., Misra S., Govinjee R., Ebrey T.* // Biochem. 2001. V. 66. P. 1588–1608 (In Russian).

58. *Sheikh S. P., Zvyaga T. A., Lichtarge O., Sakmar T. P., Bourne H. R.* // Nature. 1996. V. 383. P. 347–350.

59. *Farahbakhsh Z., Hideg K., Hubbell W.* // Science. 1993. V. 262. P. 1416–1419.

60. *Hubbell W., Cafiso D., Altenbach C.* // Nat. Struct. Biol. 2000. V. 7. P. 735–739.

61. *Altenbach C., Klein-Saathezaraman J., Cai K., Khorana H. G., Hubbell W. I.* // Biochem. 2001. V. 40. P. 1549–15500.

62. MOE (Molecular Operating Environment). http://www.chemcomp.com (used within 2002–2003, by license of CAL RIKEN).

63. *Case D. A., Pearlman D. A., Caldwell J. W., Cheatham (III) T. E., Ross W. S., Simmerling C. L., Darden T. A., Merz K. M., Stanton R. V., Cheng A. L., Vincent J. J., Crowley M., Ferguson D. M., Radmer R. J., Seibel G. L., Singh U. C., Weiner P. K., Kollman P. A.* AMBER 5. University of California, 1997.

64. *Narumi T., Susukita R., Ebisuzaki T., McNiven G., Elmegreen B.* // Molecular Simulation. 1999. V. 21. P. 401–408.

65. *Narumi T., Susukita R., Furusawa H., Ebisuzaki T.* // Proc. of the 5th Int. Conf. on Signal Processing. Beijing, 2000. P. 575–582.

66. *Okimoto N., Yamanaka K., Suenaga A., Hirano Y., Futatsugi N., Narumi T., Yasuoka K., Susukita R., Koishi T., Furusawa H., Kawai A., Hata M., Hoshino T., Ebisuzaki T.* // Chem.-Bio. Inform. J. 2003. V. 3, No.1. P. 1–11.

67. *Cornell W. D., Cieplak P., Bayly C. I., Gould I. R., Merz K. M. (Jr.), Ferguson D. M., Spellmeyer D. C., Fox T., Caldwell J. W., Kollman P. A.* // J. Am. Chem. Soc. 1995. V. 117. P. 5179–5197.

68. *Jorgensen W. L., Chandrasekhar J., Madura J. D.* // J. Chem. Phys. 1983. V. 79. P. 926–935.

69. *Berendsen H. J. C., Postma J. P. M., van Gunsteren W. F., DiNola A., Haak J. R.* // J. Chem. Phys. 1984. V. 81. P. 3684–3690.

70. *Ryckaert J. P., Ciccotti G., Berendsen H. J. C.* // J. Comp. Phys. 1997. V. 23. P. 327–341.

71. *Sayle R. A., Milner-White E. J.* RasMol: Biomolecular Graphics for All. // Trends in Biochem. Sci. 1995. V. 20. P. 374–376.

72. *Koradi R., Billeter M., Wüthrich K.* MOLMOL: A Program for Display and Analysis of Macromolecular Structure // J. Mol. Graph. 1996. V. 4. P. 51–55.

73. *Kim J., Altenbach C., Thurmond R., Khorana H. G., Hubbell W. I.* // Proc. of the Nat. Acad. Sci. USA. 1997. V. 94. P. 14273–14278.

74. *Franke R., Konig B., Sakmar T., Khorana H.* // Science. 1990. V. 250. P. 123–125.

75. *Fahmy et al.* // Proc. of the Nat. Acad. Sci. USA. 1993. V. 90. P. 10206–10210.

Received on March 2, 2005.

Корректор *Т. Е. Попеко*

Подписано в печать 6.06.2005.
Формат 60 × 90/16. Бумага офсетная. Печать офсетная.
Усл. печ. л. 2,18. Уч.-изд. л. 3,08. Тираж 220 экз. Заказ № 54908.

Издательский отдел Объединенного института ядерных исследований
141980, г. Дубна, Московская обл., ул. Жолио-Кюри, 6.
E-mail: publish@pds.jinr.ru
www.jinr.ru/publish/